X-ray spectroscopy evidence for plasma shell formation in experiments modeling accretion columns in young stars

E. D Filippov, I. Yu. Skobelev, G. Revet, S. Chen, B. Khiar, A. Ciardi, D. Khaghani, D. P Higginson, S. Pikuz, J. Fuchs

X-ray spectroscopy evidence for plasma shell formation in experiments modeling accretion columns in young stars

E.D. Filippov[1,a)], I.Yu. Skobelev[1,2], G.Revet[3], S.N. Chen[4], B. Khiar[5,6], A. Ciardi[5], D. Khaghani[7], D.P. Higginson[8], S.A. Pikuz[1,2] and J. Fuchs[3].

AFFILATIONS:

[1] *Joint Institute for High Temperatures, RAS, 125412, Moscow, Russia.*

[2] *National Research Nuclear University "MEPHI", 115409, Moscow, Russia.*

[3] *LULI-CNRS, École Polytechnique, CEA: Université Paris-Saclay, UPMC Univ Paris 06: Sorbonne Université; F-91128 Palaiseau cedex, France.*

[4] *ELI-NP, "Horia Hulubei" National Institute for Physics and Nuclear Engineering, 30 Reactorului Street, RO-077125, Bucharest-Magurele, Romania*

[5] *Sorbonne Université, Observatoire de Paris, Université PSL, CNRS, LERMA, F-75005, Paris, France*

[6] *Flash Center for Computational Science, University of Chicago, 5640 S. Ellis Avenue, Chicago, IL 60637, USA*

[7] *University of Bordeaux, CEA, CNRS, Centre Lasers Intenses et Applications, UMR 5107, 33405, Talence Cedex, France*

[8] *Lawrence Livermore National Laboratory, Livermore, CA 94551, USA*

[a)] Author to whom correspondence should be addressed: edfilippov@ihed.ras.ru

ABSTRACT

Recent achievements of laboratory astrophysics experiments with high power lasers have allowed progress in our understanding of the early stages of star formation. In particular, we have recently demonstrated the possibility of simulating in the laboratory the process of accretion of matter on young stars (Revet G. et al. Science Advances **3**, e1700982 (2017)). The present paper focuses on X-ray spectroscopy methods allowing us to investigate the complex plasma hydrodynamic involved in such experiments. We demonstrate that we can henceforth infer the formation of a plasma shell, surrounding the accretion column at the location of impact with the stellar surface, and thus resolve the present discrepancies between mass accretion rates derived from x-ray and optical radiation astronomical observations originating from the same object. In our experiments, the accretion column is modelled by having a collimated narrow (1 mm diameter) plasma stream first propagate along the lines of large-scale external magnetic field and then impact onto an obstacle mimicking the high-density region of the stellar chromosphere. A combined approach using steady-state and quasi-stationary models was successfully applied to measure the parameters of the plasma all along its propagation, at the impact and in the subsequent structure surrounding the impact region. The formation of a hot plasma shell surrounding the denser and colder core formed by the incoming stream of matter is observed near the obstacle using x-ray spatially resolved spectroscopy.

I. INTRODUCTION

Nowadays laser plasma is an excellent tool to simulate various magnetized supersonic and hydrodynamic flows[1–3]. Recently, for example, collimated long-scaled plasma streams were used in experiments to simulate jets in Young Stellar Objects (YSO)[4]. In these laboratory experiments, the most interesting processes occur far away from the laser-irradiated surface of the source target, when the plasma is no longer heated by the laser. Therefore, the common steady–state models used to analyse x-ray spectroscopy observations are not relevant and new models geared towards recombining plasmas[5] are actively being developed. This new method of x-ray spectroscopy was applied in the investigation of magnetized supersonic flows and have shown remarkable results[6].

The combination of external magnetic fields and laser-produced plasmas[6,7] allowed us to create a stable, collimated plasma stream which, in turn, let us investigate more complicated hydrodynamic phenomena. For example, this setup can be exploited to investigate the impact of a magnetized plasma column with an additional medium, e.g. gas jet, solid obstacle, another plasma etc. In particular, it has allowed us[8], by placing a solid obstacle on the path of the plasma column, as seen in Fig.1, to simulate the astrophysical processes related to matter accretion onto a young star[9,10].

The purpose of this paper is to describe the new approach of x-ray diagnostics we used in such experiments and that were recently applied successfully for the tasks of laboratory simulation of magnetized accretion columns[8].

II. EXPERIMENTAL SETUP AND MEASURED DATA

The experiments dedicated to the study of accretion dynamics in Classical T Tauri Stars (CTTSs)[11] were performed at the nanosecond laser facility ELFIE at Ecole Polytechnique (France). The experimental platform was described in details in Ref. 6 and is shown in Figure 1. A narrow, ~ 1 mm diameter, and cm-long collimated jet has been created by the interaction of a laser beam with a solid thick target in the presence of poloidal uniform large-scale magnetic field ~ 20 T[4,6]. As a result, the plasma jet evolves parallel to the lines of magnetic field and is made to interact with a solid obstacle mimicking the region of a stellar chromosphere (see Fig.1).

The plasma flow strongly emits in a wide x-ray spectral range and so x-ray spectroscopy methods can be properly used for the investigation of plasma expansion as described in Refs 5,12,13. CF_2 (Teflon) targets with a low mean atomic number Z ($Z_{mean} = 8$) were chosen in respect of the given laser intensity on target (~10^{13} W/cm^2), thus creating an almost fully ionized plasma. The focusing spectrometer (FSSR) which is based on a spherically bent mica crystal with $2d = 19.9376$ Å and a radius of curvature $R = 150$ mm was used to analyze the x-ray emission stemming from the plasma. For this particular setup, the FSSR was implemented to measure x-ray spectra of multi-charged ions of

Fluorine in the range of 13–16 Å (800–950 eV) in the first order of reflection (see Fig.2). The spectrometer was installed in the direction transverse to the jet expansion providing a spatial resolution of about 350 μm over more than 12 mm distance along the jet.

with a slight angle in the upwards (~ 5°) and lateral (~ 2°) directions, which were small enough to for us to neglect the skewing of the image. This arrangement allowed us to use it in parallel to an optical interferometer of Mach-Zehnder type, which was used to provide complementary data about the plasma dynamics, looking at the plasma electron density[8]. The x-ray spectra were recorded on a fluorescent detector, the TR Fujifilm Image Plate.

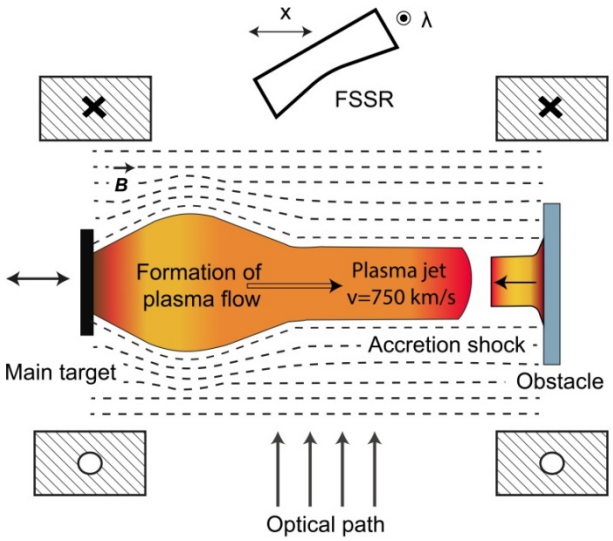

Fig.1: Scheme (top view) of the creation of a collimated plasma stream in the laboratory (on the left) that is used to simulate the formation of accretion column (on the right). Here the main target is irradiated by a pulsed laser (0.6 ns / 1054 nm / 40 J) and then the created plasma jet hits the solid obstacle that is used to generate accretion shocks. A magnetic field, generated by a Helmholtz coil[6], is applied uniformly everywhere to collimate the plasma flow[4,6]. The targets could be shifted compared to the central transverse observation hole managed in the middle of the coil system in order to observe all the expansion dynamics of the jet[4,6]. Optical and x-ray measurements (the Focusing Spectrometer with Spectral Resolution, or FSSR) are provided in the transverse direction using that observation hole. The FSSR provides spatial resolution along all the plasma expansion axis, as well as spectral resolution in the 13-16 Å range.

Typical spectral images measured in the experiment are presented in Fig.2. The emission is composed of Bremsstrahlung and the following spectral components of Fluorine ions: Helium-like ion emission starting with transition 3p-1s (He_β line) and Hydrogen-like ion emission with Ly_α line and its dielectronic satellites. One can observe that the spectra change significantly as a function of the distance to the surface of the laser irradiated target and as the plasma flow expands for many millimeters and tens of ns from laser-interaction volume. We observe dielectronic satellites to the Ly_α

line near the laser-irradiated target. Here the plasma temperature is sufficient to ionize inner ion shells. Further, i.e. at > 1 mm from the target surface, the absolute intensities of spectral lines decrease and the satellites disappear. In this remote region, the contribution of He-like transitions from the level with a larger main quantum number increases in the total spectrum, which is typical of a recombining plasma[14]. Then, near the obstacle surface, the absolute line intensities increase again and satellites to the Ly_α line are well distinguished, while the behavior of He-like ion emission is preserved.

The Doppler shift is negligible and not observed in the experimental spectrum. Note that, since the plasma flow propagates laterally with respect to the observer (fig.1), only transverse Doppler shift could arise. This would yield a spectral shift of less than 10^{-4} Å for the plasma velocities measured in the experiment, which are in the range 100-1000 km/s[8]. For the later stages of plasma expansion when the longitudinal Doppler shift may affect the spectral lines broadening, plasma velocity is estimated to be even lower and so the total broadening is less than the instrumental line width.

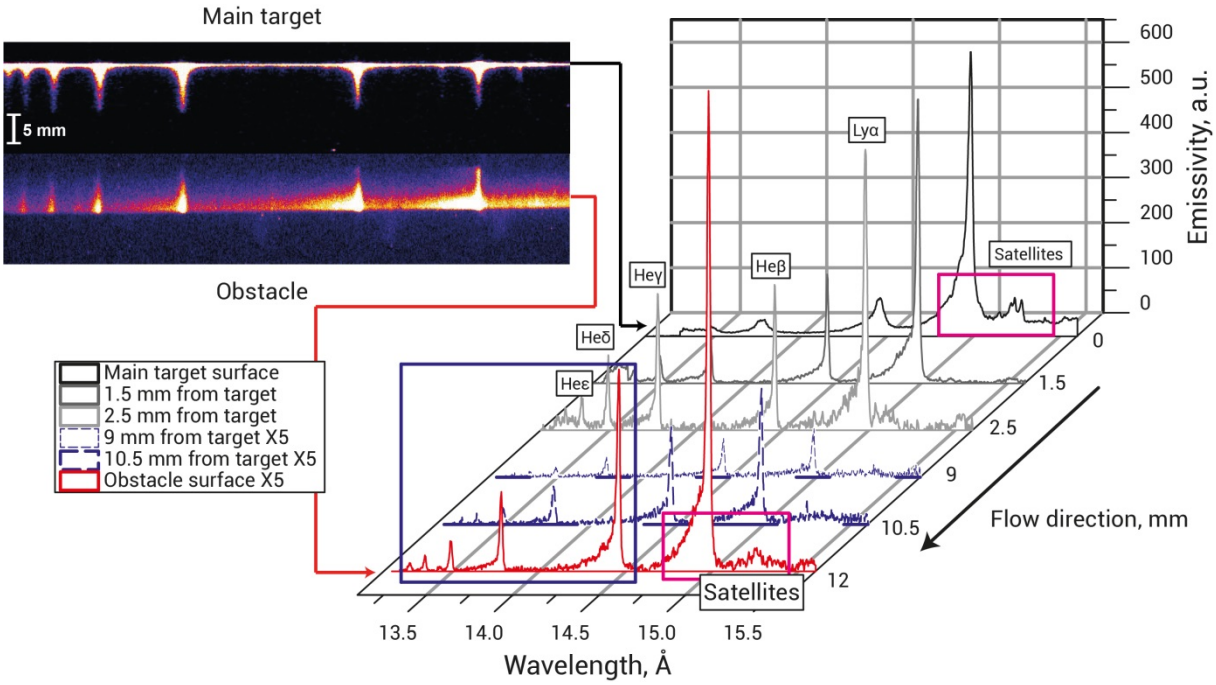

Fig.2: Top images: Measured raw data close to the main and obstacle targets; the horizontal axis is the spectral one, while the vertical axis is the one along which the main plasma expansion occurs. Also shown are spectra of Fluorine lines at different distances from the laser irradiated surface of the main target, using the FSSR spectrometer. The observed spectral components that can be used for simulating the plasma parameters are the He-series (starting with transition 3p-1s, as highlighted in the blue box) and the Ly_α line of Fluorine with its dielectronic satellites (as highlighted in the pink box).

Although the signal on the detector is integrated over time, in the case of a free plasma expansion (i.e. no obstacle) the flow moves with constant velocity (i.e. all acceleration processes are

supposed to occur only close to the target surface) along the spatially-resolved axis, and a quite good correspondence can be made between the spatial scale and temporal evolution of the plasma parameters. However, in the case when a solid obstacle is put on the way of a plasma plume, actually, each spatial point of data measured by spectrometer should be considered as the sum of spectra emitted, firstly, by the laser-initiated plasma spreading towards the obstacle and, secondly, by the plasma formed after impact of this plasma outflow on the obstacle surface. In the experiment, the ion emission when the plasma is freely propagating (i.e. in the absence of obstacle) is noticeably lower compared to the emission when the plasma impacts on the solid obstacle. It means that the plasma emission is formed close to the obstacle mainly following the impact of the plasma stream on the obstacle surface.

In addition, the plasma near the obstacle consists of ions generated from both the main and obstacle targets, hampering to clearly distinguish their respective ion emission. One way to circumvent this issue is to use different target materials for the main and obstacle targets, such that the ions from both materials emit in different spectral range, which allows thus to separate their emissions. This was what was done in our experiment, using CF_2 for one target, and polyvinyl chloride [PVC $(C_2H_3Cl)_n$] for the other[8].

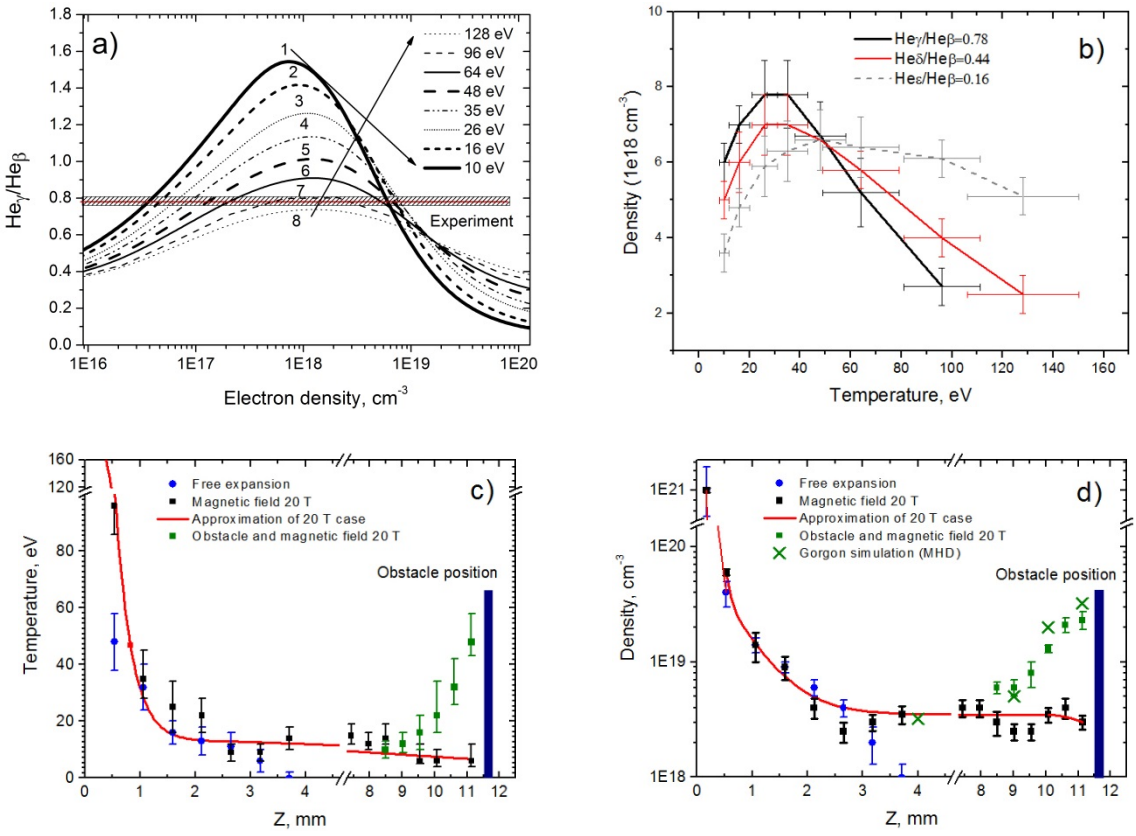

Fig. 3: (a) Simulation of the intensity ratio for the lines He_β and He_γ using our recombination model, for different values of the plasma density and temperature, compared to the experimental value of the same ratio

recorded for the plasma jet stemming from the main target, i.e. the part of the plasma recorded at Z=1 mm from a laser-irradiated target. One can remark that there can be, for one plasma electron temperature, two sets of solutions, one at low density ($<10^{18}$ cm^{-3}), one at higher density. The solutions at low density are discarded since they are not consistent with neither the density retrieved from the optical interferometric measurement, nor the hydrodynamic simulations[4,6]. (b) Solution curves in a T_e/N_e map for experimentally observed values of He_γ/He_β=0.78, He_δ/He_β=0.44 and He_ε/He_β=0.16 in the experiment (i.e. corresponding to the same plasma conditions at d=1 mm from the main target) and as obtained through similar calculations as those shown in (a). One can observe that using these three ratios allows to narrow down the retrieved plasma parameters to a single solution in electron density and temperature. Here it corresponds to ~ T_e = 50 eV and $N_e = 6.5 \cdot 10^{18}$ cm^{-3}. (c, d) Applying the same procedure at all points in the plasma along its expansion, spatial profiles of electron temperature T_e and density N_e can thus be retrieved for the cases of free propagation (no obstacle and magnetic field, blue dots), then for the case of jet expansion within the poloidal magnetic field of 20 T strength, with the magnetic field lines parallel to plasma expansion (black squares), and finally for the case of the impact on the obstacle surface, still magnetized using a 20 T magnetic field (green squares). As well, we give here the MHD simulation values for the electron density (green crosses) performed by the code Gorgon[20] for the core plasma component (see below). For the shell plasma, Gorgon gives N_e=1–5·10^{18} cm^{-3} near the obstacle.

III. DATA ANALYSIS

The absolute and relative intensities of several spectral lines belonging to different charge states of ions, such as the ones shown in Fig.2, can be used to retrieve the plasma parameters (electron temperature, density etc.) along all the plasma expansion and to unfold the whole scenario of the plasma-obstacle interaction.

First, one can observe that the most intense emission is located near the laser-irradiated target, since that plasma is characterized by the highest electron density, i.e. the critical density where the laser-matter interaction takes place, with $N_e \sim 10^{21}$ cm^{-3}. The possibility of simultaneously observing the resonance lines of multiply charged K-ions and their satellites in this region is a consequence of the population and decay processes for the resonance and autoionizing levels. The satellites are initiated here by dielectronic recombination from the doubly excited states of ions which are situated very close to the corresponding resonance line (Ly_α in this case). They proved[15,16] to be an effective method of plasma diagnostics, since the satellite-to-resonance-line intensity ratio is essentially dependent on the temperature and in some cases on the electron density. In a previous experiment conducted with identical parameters of laser and target[17], the temperature ~ 300 eV was measured at the target surface in a steady-state plasma approach. Calculations to support inferring such temperature were performed using the "zero-dimensional" program code FLYCHK[12] which features a collisional-radiative model.

Second, we note that the ion emission of the expanding plasma has a recombination behavior[14] in the regions that are remote from the target surface. Here, at a distance > 1 mm, ionization processes are negligible and the relative intensities of the He-like spectral lines are changed due to the strong dependence of the population coefficients on the plasma parameters as illustrated in Fig.3.a. In general, this regime is time-dependent and not steady-state but the quasi-stationary approach[5] is commonly applied to measure the plasma parameters. It is based on the calculation of the relative intensities of spectral lines for ions having the same charge state (see Fig.3a). The method is sensitive to densities in the range of 10^{16}–10^{20} cm^{-3} when the temperature ranges from 10 to 100 eV for ions with Z ~ 10; note that here we suppose that the ion mean charge is "frozen". Here the relative intensities of the $1snp\ ^1P_1 - 1s^2\ ^1S_0$ transitions in Fluorine ions, where $n = 3 - 7$ (He$_\beta$, Heγ, He$_\delta$, He$_\varepsilon$, He$_\xi$ lines correspondingly), were considered. Despite of a certain error in the measurement of intensity ratios (quantified by the width of the bar in Fig.3.a), the utilization of several ratios inside the He-like ion series makes it possible to unambiguously determine the electron temperature and density at any point along the plasma expansion, as illustrated in Fig.3.b. Finally, the retrieved plasma parameters for the plasma expanding from the main target are summarized in Fig.3.c-d.

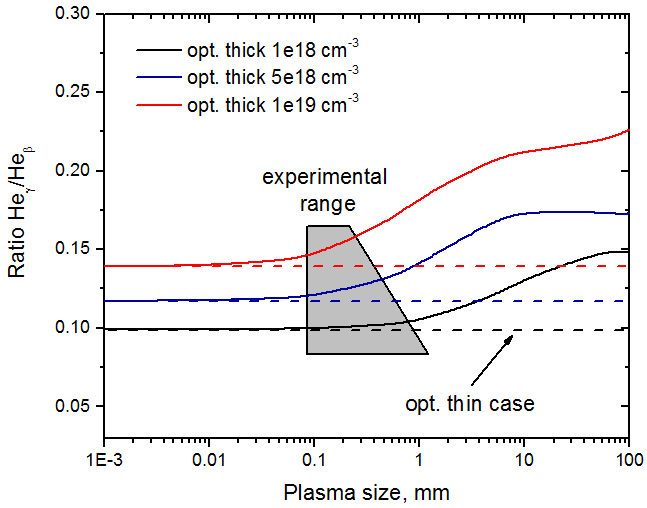

Fig. 4: Ratio of the spectral intensities of the Heγ/He$_\beta$ lines for Fluorine versus plasma size in the radiative-collisional code FLYCHK at 100 eV and for variable (10^{18}, $5\cdot10^{18}$, 10^{19} cm^{-3} respectively) electron density for optically thin and optically thick plasmas. Overlaid is shown the experimentally measured (using optical interferometry) range of plasma size for the considered ratios.

Note that, in order to apply this quasi-stationary approach, the plasma must be optically thin in the laboratory conditions. An estimation of the influence of the optical depth on the intensity of the ion emission can be provided by means of the comparison of the relative intensities of the $1snp\ ^1P_1 - 1s^2\ ^1S_0$ transitions in Fluorine ions for optically thin and optically thick plasmas, while varying the

plasma size in the simulation, as illustrated in Fig.4. In the optically thin case, the ratios of the corresponding spectral lines do obviously not depend on the plasma thickness. Fig. 4 gives the simulated ratio of the intensities of the spectral lines He_β and He_γ in a plasma at $T_e \sim 100$ eV and having a variable density, corresponding to typical values recorded in the experiment in the case of a recombining plasma, i.e. far from the main target (see Fig.3.d)[17]. These calculations are made for various lateral plasma size, using FLYCHK code and in the cases of optical thin (dashed lines) and thick plasmas (solid lines). On top of this, the experimentally measured range for the considered ratio is shown. In the experiment, the optical measurements allows[4,6] us to assess that the lateral size of the recombining plasma is about 1 mm for a density $\sim 10^{18}$ cm^{-3}. As a consequence, what can be observed in Fig.4 is that the measured ratio is quite consistent with the one calculated in the hypothesis of an optically thin plasma. Hence, this tends to give support to the optically thin plasma hypothesis for the hereby considered recombining plasma.

In Fig.3.c-d, one observes a fast decrease of T_e, N_e along the expansion axis in the case when no magnetic field is applied (blue dots). Conversely, in the case where we apply a magnetic field of 20 T strength (black dots), the initially heated plasma flow maintains far from the main target, i.e. at distances > 2 mm, almost constant values of electron temperature and density, i.e. $T_e \sim 20$ eV and $N_e \sim 4 \cdot 10^{18}$ cm^{-3} respectively. Later on, in the case where an obstacle is put in the way of the plasma propagation (green dots), we observe a substantial increase of the electron temperature and density up to 50 eV and $2 \cdot 10^{19}$ cm^{-3} in the region near the obstacle.

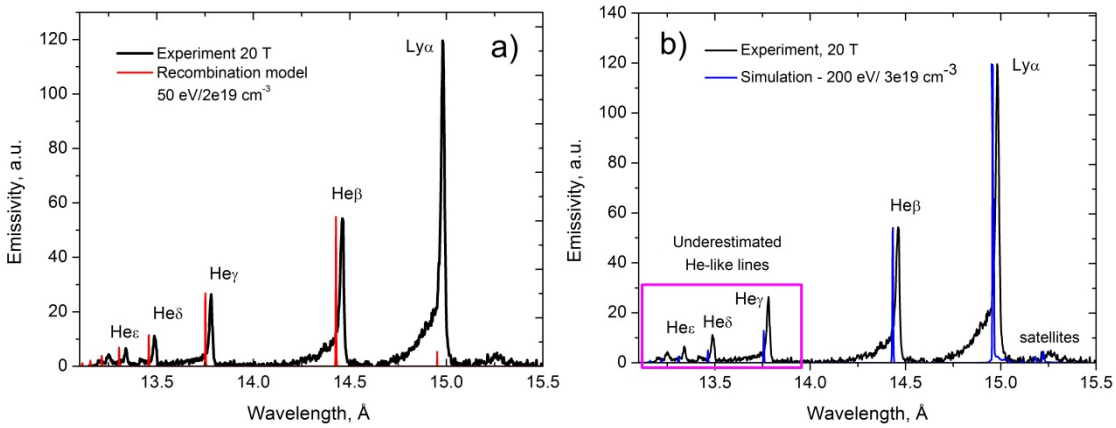

Fig.5: (a) Simulation (red lines) of the experimental spectrum (black curve) by a quasi-stationary recombining model with parameters T_e=50 eV and N_e=$2 \cdot 10^{19}$ cm^{-3}, (b) Simulation (blue lines) of the experimental spectrum (black curve) using a collisional-radiative one-temperature model in the FLYCHK code. Note that in the model, the intensities of He-like transitions are clearly underestimated compared to what the measurements show. The experimental spectrum is recorded at the surface of the obstacle, and corresponds to the configuration in which the setup is magnetized with strength of 20 T. Also note, the spectral lines in the simulation are specially shifted in wavelengths for more convenient comparison with experimental data.

To retrieve the plasma parameters in the case when a solid unheated obstacle is put on the way of the recombining plasma, one has to carefully consider that the shock formation and plasma heating at the location of the obstacle can lead to an additional excitation of ions. Typically, this implies higher temperatures ($T_e >> 100$ eV, exceeding the ionization potential for L-shell) and higher densities than in free propagation case[18,19]. Then the recombination approach is not applicable alone anymore and an additional contribution to the kinetic model by ionization should be taken into account. Fig. 5.a demonstrates the sudden appearance of a strong Ly_α line as well as satellites near the obstacle position, both of which that definitely cannot be described using solely a recombination model (as shown by the red lines in Fig. 5.a). The spectra shown here were integrated over 400 μm along the expansion axis to achieve a better signal-to-noise ratio. At the same time, as can be seen in Fig. 5.b, a simulation performed in a steady-state collisional-radiative model with a single-temperature plasma fits the experimental ratio Ly_α/He_β as well as describes the satellites nearby, but the intensities of the rest of the He-like lines with a larger main quantum number **n** are clearly underestimated. Thus, according to Fig.5.a, a reasonable assumption is to assume the presence of an additional plasma component, on top of the one modeled in Fig.5.a, and which can yield the observed strong Ly_α line. The observed x-ray emission stemming from near the obstacle surface can thus be envisioned as resulting from the overlap of two emissions originating from two different plasmas. The first emission originates from the recombining plasma coming from the main target and which has propagated up to the obstacle, while the second emission, contributing to the observed higher charge states (Ly_α and satellites), is coming from a hotter plasma generated at the obstacle surface following the impact of the expanding jet. This latter emission can be described by a pure steady-state model.

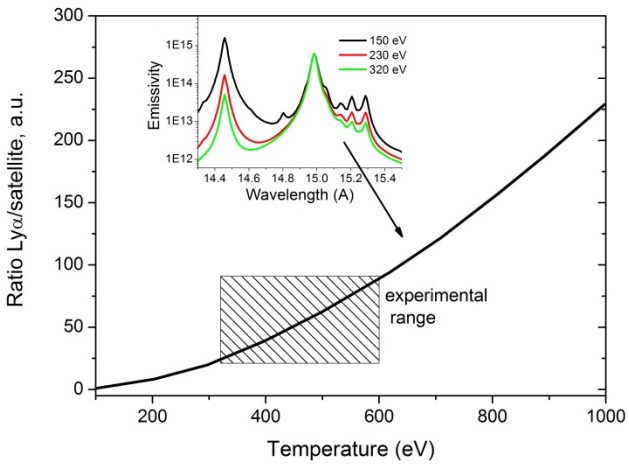

Fig.6: Simulation of the experimental Ly_α-to-satellites ratio for multi-charged ions of Fluorine and as function of the electron plasma temperature. Note that the sensitivity to the density is quite low in the range of electron densities 10^{17}-10^{20} cm^{-3}. The dielectronic satellites are located in the spectral range 15.159-

15.291 Å and the most intense of them (right one in inset) is F VIII ($2p^2$) $^1D_2$ – (1s2p) $^1P_1$. For the simulation of Ly_α/satellites ratio, the averaged profile of all three satellites was used.

Hence, the experimental spectrum was finally simulated using the following parameters (electron temperature and density) according to the experimental x-ray data: T_1 = 50 eV, N_1 = $2.3 \cdot 10^{19}$ cm^{-3} for the shocked plasma modeled in a recombining model and T_2 = (320–600) eV for the shocked plasma near the obstacle and using the simulation of Ly_α to satellites (see Fig.6) in a steady-state model. The satellites have a low intensity in the experimental data and so the method based on analyzing their relative intensity to the one of the Ly_α line has a significant error bar, which is here taken into account and which is represented in Fig.6 by the rectangular hatching. Note that this uncertainty in the measurement also hampers us in determining reliable values for the density of the second plasma component, which is why it is not quoted here.

We note that the plasma parameters inferred this way for the two components of the plasma near the obstacle surface are well consistent with the modeling obtained by simulating the experiment using the code GORGON[20] and in which we evidence the formation of a hot plasma “shell” surrounding a central, colder “core” (see Fig.7 and 3d). Here the terms "hot" and "cold" refer to the electron temperature only. The hot shell observed in the GORGON simulation is consistent with the plasma component that yields the strong Ly_α line and the associated satellites. The model used in GORGON simulation describes a two-temperature one-fluid resistive plasma which is optically thin. It was initially developed for experiments on Z-pinches but is now widely used for laboratory astrophysics laser-plasma experiments[21,22]. The formation of the hot (in terms of electron plasma temperature) shell as observed in the simulation performed using the GORGON code results from the following scenario: after the laser-induced plasma stream has impacted the obstacle, the shocked plasma escapes radially but is re-collimated on axis by the external magnetic field. This re-collimation of the plasma flow is accompanied by the heating of the electrons within the periphery regions, i.e. in the shell[8]. Indeed, within the core, there is a decoupling of the ion and electron temperatures after the shock, the ions being the ones heated by the shock. Since the electrons can be heated only through collisions after some time along their trajectories, it results that hot electrons are predominantly located in the shell.

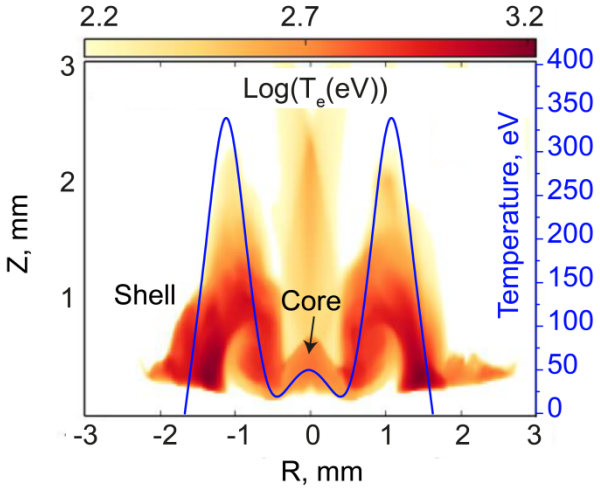

Fig.7: Color map of the electron temperature, derived by computer simulation using the GORGON code. This corresponds to the plasma near the obstacle surface (located at Z=0), as recorded 12 ns following the incoming jet impact and for a magnetic field of 20 T. Overlaid is the comparison with x-ray data derived by the FSSR spectrometer (blue curve) following the assumption that the hotter plasma is the one of the shell. Note that the right axis pertains only to the blue curve.

Thus, the x-ray spectra shown in fig. 5 describes two plasma components separated in space, one of them is a plasma shell and the other one is a plasma core. Since we have been able to already derive the parameters of the cold core, we will now focus on trying to unfold the density of the hot shell (the temperature of the latter was already inferred by the Ly_α/satellites ratio, see fig. 6). For this, we will particularly consider the ratio between the Ly_α and He_β lines in the x-ray spectra since the hydrogen and helium–like series for a given spectral range belong mostly to different plasma components. The He-like series of ion emission is emitted by the recombining plasma (i.e. the cold core), while Ly_α line is dominantly produced by the hot post-shocked zone (i.e. in the shell). The emissivity of the hot plasma can be evaluated in a wide range of electron densities (see fig. 8) by a steady-state model in FLYCHK. The emissivity of He-like emission on the other hand is defined by the quasi-stationary approach[5]. Then the experimentally observed ratio can be expressed as:

$$\left(\frac{Ly\alpha}{He\beta}\right)_{exp} = E_{Ly\alpha}(T_e, N_e) \times \frac{V_{hp}}{V_{cold}} / E_{He\beta}, \qquad (1)$$

where E is the emissivity of a spectral line, V the volume of a corresponding plasma component and the emissivity $E_{He\beta}$ is calculated by a recombination model[5]. Taking the volume ratio between the two plasma (shell/core) fractions retrieved from the interferometry data[8], it is hence possible to calculate the electron density of the hot plasma (i.e. the shell) component in the experiment being up to ~ $5 \cdot 10^{18}$ cm^{-3}.

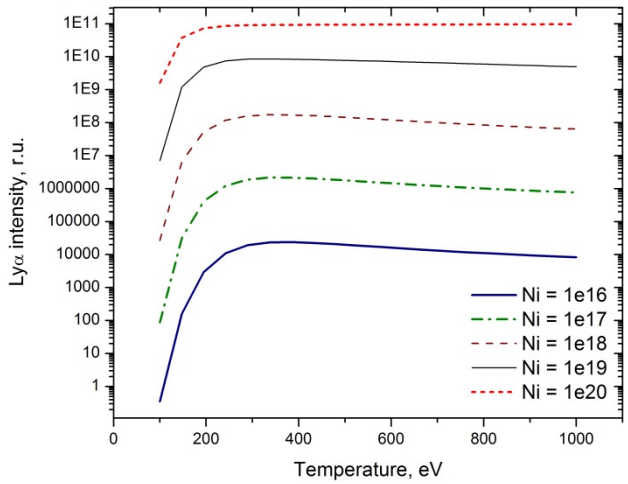

Fig.8: Simulation of the emissivity of the Ly_α line for a hot plasma component in a wide range of ion density (in units of cm^{-3}) and temperature and as calculated using the FLYCHK code. The electron density is calculated each time for a given ion density and a given temperature using kinetic equations.

The final parameters of plasma components are depicted in Table 1 for the magnetic field strengths used in the experiment, i.e. 20 and 6 T. Note that in the latter case, the analysis was performed analogously as to what has been detailed above. Here, in line with the GORGON simulations and the optical interferometry data[8], we have assumed that the hot plasma component is a shell enveloping a cold core. We can observe a significant difference between the 20 T and 6 T cases in terms of electron densities for the core plasma, up to ~ 10 times; note that such difference is fully consistent with optical interferometry data. At the same time, the electron temperature is similar for both cases. We associate this effect to additional ionization of plasma and collimation of plasma flow when the magnetic field is applied. This leads to the increase in plasma density and faster recombination rate making it possible to measure the electron density by our technique.

B field, T	**T_{core}, eV**	**N_{core}, cm^{-3}**	**T_{shell}, eV**	**N_{shell}, cm^{-3}**
20	50	$2.3 \cdot 10^{19}$	320–600	$3.8–4.9 \cdot 10^{18}$
6	40	$3.3 \cdot 10^{18}$	320–600	$3.7–4.6 \cdot 10^{17}$

Table 1: X-ray spectroscopy-retrieved parameters of the two plasma components that could be identified in the experiment simulating accretion phenomena of young stars for strengths 20 T and 6 T of the externally applied magnetic field. Here T_{core} and T_{shell} correspond to electron temperature, N_{core} and N_{shell} – to electron density for both core and shell plasmas.

For the shell, its optical depth can be evaluated in FLYCHK, similarly as what was done for the recombining plasma (i.e. the core) as presented in Fig.4. The value of optical depth is found here to be $\tau \sim 0.3$, validating a posteriori the possibility to use the Ly_α to He_β ratio for evaluating the shell plasma

parameters. Even though we note that the shell revealed in the experiment is optically thin, we have to note that this is not necessarily the case in the astrophysical case. i.e. the transport of x-ray emission is not scalable from the laboratory to the astrophysical case. For example, a strong emission in the x-ray and UV ranges is suggested to take place following the impact of accretion columns on young stellar objects due to the high temperature induced in the shocked plasma[23]. But last astrophysical observations[24,25] have shown that the mass accretion rates are different for calculations based on x-ray and optical range of radiation. The effect of the optical depth in x-ray range is given as one of possible reasons. The explanation can be also found in Ref. 26 where the idea of "accretion-fed corona" is presented. In that case the x-ray emission originates from three plasma components: a hot corona, a high density post-shock region close to the shock front, and a cold less dense post-shock cooling region. We stress here that in the astrophysical case[26], the situation, in terms of electron temperature, is the reverse of the one observed in the laboratory experiment, namely one of a cold shell surrounding a hot core. This is due to the very short equilibration time between ions and electrons in the astrophysical case compared to the time-scale of the hydrodynamic shell formation, when on the contrary in the laboratory experiment, the shell formation takes place on short time-scales than the ions and electrons equilibration. Hence, the formation of a cold shell plasma, highlighted here in laboratory experiments, could in the astrophysical case potentially lead to x-ray absorption of the emission originating from the hot core, with a direct influence on the calculated mass accretion rate.

IV. CONCLUSIONS

We developed a combined approach to characterize the dynamics of a magnetized plasma flow when it collides with a solid obstacle, mimicking the formation of accretion columns in young stars. The approach is based on the simulation of the relative intensities of x-ray spectral lines emitted by differently charged states of ions. On top of the plasma flow colliding onto the obstacle, henceforth a shock develops in which the ions are first heated, and hence the electrons stay relatively cold, we suppose the generation of an additional, hotter, plasma component that results from the expansion into vacuum of the plasma escaping from the shock region. That second plasma component induces a significant x-ray emission from higher charge states, i.e. the Ly_α line and its dielectronic satellites. The ratio between the emitted Ly_α and He_β lines in the x-ray region was successfully used to derive the localization of these two plasma components since these two lines are predominantly emitted by, respectively, the hotter (post-shock) and colder (shocked) plasma components. Overall, this leads to the evidence for the formation of a hot plasma shell with $T_e > 320$ eV enveloping a cold dense core with $T_e \sim 50$ eV and $N_e \sim 2 \cdot 10^{19}$ cm^{-3}. These plasma parameters are consistent with numeric simulations performed by the magnetohydrodynamic code GORGON and with optical interferometry

measurements of the same plasma[8]. The formation of shell plasma in the astrophysical case could lead to substantial absorption of x-ray emission of accretion columns generated in YSO[8].

ACKNOWLEDGEMENTS

X-ray data measurement, modeling and analysis are made by JIHT RAS team under financial support of Russian Science Foundation (project #17-72-20272). The authors thank the entire staff of the ELFIE laser facility at LULI for their support during the experimental preparation and execution. This work was supported by ANR Blanc Grant No. 12-BS09-025-01 SILAMPA. It has received funding from the European Union's Horizon 2020 research and innovation programme through the European Research Council (ERC, grant agreement No 787539). It was partly done within the LABEX Plas@Par project, which is supported by Grant No. 11-IDEX-0004-02 from Agence Nationale de la Recherche. The research leading to these results is supported by Extreme Light Infrastructure Nuclear Physics (ELI-NP) Phase I, a project co-financed by the Romanian Government and European Union through the European Regional Development Fund.

REFERENCES

[1] G.Y. Liang, J.Y. Zhong, H.G. Wei, D.W. Yuan, Z. Zhang, C. Wang, B. Han, B.J. Zhu, W.M. Jiang, J.M. Peng, T. Tao, G.Y. Hu, F.L. Wang, X. Gao, B.Q. Zhu, J.Q. Zhu, X.W. Ma, Y.T. Li, G. Zhao and J. Zhang. Laboratory Analog of Heavy Jets Impacting a Denser Medium in Herbig–Haro (HH) Objects. Astrophys. J. **868**, 56 (2018).

[2] C.K. Li, P. Tzeferacos, D. Lamb, G. Gregori, P.A. Norreys, M.J. Rosenberg, R.K. Follett, D.H. Froula, M. Koenig, F.H. Seguin, J.A. Frenje, H.G. Rinderknecht, H. Sio, A.B. Zylstra, R.D. Petrasso, P.A. Amendt, H.S. Park, B.A. Remington, D.D. Ryutov, S.C. Wilks, R. Betti, A. Frank, S.X. Hu, T.C. Sangster, P. Hartigan, R.P. Drake, C.C. Kuranz, S. V Lebedev and N.C. Woolsey. Scaled laboratory experiments explain the kink behaviour of the Crab Nebula jet. Nat. Commun. **7**, 13081 (2016).

[3] C.M. Krauland, R.P. Drake, C.C. Kuranz, R. Sweeney, M. Grosskopf, S. Klein, R. Gillespie, P.A. Keiter, B. Loupias and E. Falize. Radiative reverse shock laser experiments relevant to accretion processes in cataclysmic variables. Phys. Plasmas **20**, (2013).

[4] B. Albertazzi, A. Ciardi, M. Nakatsutsumi, T. Vinci, J. Beard, R. Bonito, J. Billette, M. Borghesi, Z. Burkley, S.N. Chen, T.E. Cowan, T. Herrmannsdorfer, D.P. Higginson, F. Kroll, S.A. Pikuz, K. Naughton, L. Romagnani, C. Riconda, G. Revet, R. Riquier, H.-P.H.-P. Schlenvoigt, I.Y. Skobelev, A.Y.Y. Faenov, A. Soloviev, M. Huarte-Espinosa, A. Frank, O. Portugall, H. Pepin, J. Fuchs, J. Béard, R. Bonito, J. Billette, M. Borghesi, Z. Burkley, S.N. Chen, T.E. Cowan, T. Herrmannsdörfer, D.P. Higginson, F. Kroll, S.A. Pikuz, K. Naughton, L. Romagnani, C. Riconda, G. Revet, R. Riquier, H.-

P.H.-P. Schlenvoigt, I.Y. Skobelev, A.Y.Y. Faenov, A. Soloviev, M. Huarte-Espinosa, A. Frank, O. Portugall, H. Pépin and J. Fuchs. Laboratory formation of a scaled protostellar jet by coaligned poloidal magnetic field. Science. **346**, 325 (2014).

[5] S.N. Ryazantsev, I.Y. Skobelev, A.Y. Faenov, T.A. Pikuz, A.N. Grum-Grzhimailo and S.A. Pikuz. X-ray spectroscopy diagnostics of a recombining plasma in laboratory astrophysics studies. JETP Lett. **102**, 707 (2015).

[6] D.P. Higginson, G. Revet, B. Khiar, J. Béard, M. Blecher, M. Borghesi, K. Burdonov, S.N. Chen, E. Filippov, D. Khaghani, K. Naughton, H. Pépin, S. Pikuz, O. Portugall, C. Riconda, R. Riquier, S.N. Ryazantsev, I.Y. Skobelev, A. Soloviev, M. Starodubtsev, T. Vinci, O. Willi, A. Ciardi and J. Fuchs. Detailed characterization of laser-produced astrophysically-relevant jets formed via a poloidal magnetic nozzle. High Energy Density Phys. **23**, 48 (2017).

[7] D.P. Higginson, P. Korneev, J. Béard, S.N. Chen, E. D'Humières, H. Pépin, S. Pikuz, B. Pollock, R. Riquier, V. Tikhonchuk and J. Fuchs. A novel platform to study magnetized high-velocity collisionless shocks. High Energy Density Phys. **17**, 190 (2015).

[8] G. Revet, S.N. Chen, R. Bonito, B. Khiar, E. Filippov, C. Argiroffi, D.P. Higginson, S. Orlando, J. Béard, M. Blecher, M. Borghesi, K. Burdonov, D. Khaghani, K. Naughton, H. Pépin, O. Portugall, R. Riquier, R. Rodriguez, S.N. Ryazantsev, I. Yu. Skobelev, A. Soloviev, O. Willi, S. Pikuz, A. Ciardi and J. Fuchs. Laboratory unraveling of matter accretion in young stars. Sci. Adv. **3**, e1700982 (2017).

[9] S. Scaringi, T.J. Maccarone, E. Kording, C. Knigge, S. Vaughan, T.R. Marsh, E. Aranzana, V.S. Dhillon and S.C.C. Barros. Accretion-induced variability links young stellar objects, white dwarfs, and black holes. Sci. Adv. **1**, e1500686 (2015).

[10] A. Caratti O Garatti, B. Stecklum, R. Garcia Lopez, J. Eislöffel, T.P. Ray, A. Sanna, R. Cesaroni, C.M. Walmsley, R.D. Oudmaijer, W.J. De Wit, L. Moscadelli, J. Greiner, A. Krabbe, C. Fischer, R. Klein and J.M. Ibañez. Disk-mediated accretion burst in a high-mass young stellar object. Nat. Phys. **13**, 276 (2017).

[11] S. Orlando, G.G. Sacco, C. Argiroffi, F. Reale and A. Maggio. X-ray emitting MHD accretion shocks in classical T Tauri stars. Case for moderate to high plasma-beta values. Astron. Astrophys. **510**, A71 (2010).

[12] H.K. Chung, M.H. Chen, W.L. Morgan, Y. Ralchenko and R.W. Lee. FLYCHK: Generalized population kinetics and spectral model for rapid spectroscopic analysis for all elements. High Energy Density Phys. **1**, 3 (2005).

[13] J.J. MacFarlane, I.E. Golovkin, P.R. Woodruff, D.R. Welch, B. V Oliver, T.A. Mehlhorn and R.B. Campbell. Simulation of the ionization dynamics of aluminum irradiated by intense short-pulse lasers. Proc. Inert. Fusion Sci. Appl. (American Nucl. Soc. La Grange Park. IL) 1 (2003).

[14] A.Y. Faenov, I.Y. Skobelev and F.B. Rosmej. High resolution X-ray spectroscopy of laser generated plasmas. in *Phys. Scr. T* (1999).

[15] A.H. Gabriel. Dielectronic Satellite Spectra for Highly-Charged Helium-Like Ion Lines. Mon. Not. R. Astron. Soc. **160**, 99 (1972).

[16] B. Han, F. Wang, J. Zhong, G. Liang, H. Wei, D. Yuan, B. Zhu, F. Li, C. Liu, Y. Li, J. Zhao, Z. Zhang, C. Wang, J. Xiong, G. Jia, N. Hua, J. Zhu, Y. Li, G. Zhao and J. Zhang. Measurement and analysis of K-shell lines of silicon ions in laser plasmas. High Power Laser Sci. Eng. **6**, e31 (2018).

[17] E.D. Filippov, S.A. Pikuz, I.Y. Skobelev, S.N. Ryazantsev, D.P. Higginson, D. Khaghani, G. Revet, S.N. Chen and J. Fuchs. Parameters of supersonic astrophysically-relevant plasma jets collimating via poloidal magnetic field measured by x-ray spectroscopy method. in *J. Phys. Conf. Ser.* (2016).

[18] I.L. Beigman, P.Y. Pirogovskiy, L.P. Presnyakov, A.P. Shevelko and D.B. Uskov. Interaction of a laser-produced plasma with a solid surface: soft X-ray spectroscopy of high-Z ions in a cool dense plasma. J. Phys. B At. Mol. Opt. Phys. **22**, 2493 (1989).

[19] M.A. Mazing, P.Y. Pirogovskiy, A.P. Shevelko and L.P. Presnyakov. Interaction of a laser-produced plasma with a solid surface. Phys. Rev. A **32**, 3695 (1985).

[20] A. Ciardi, S. V. Lebedev, A. Frank, E.G. Blackman, J.P. Chittenden, C.J. Jennings, D.J. Ampleford, S.N. Bland, S.C. Bott, J. Rapley, G.N. Hall, F.A. Suzuki-Vidal, A. Marocchino, T. Lery and C. Stehle. The evolution of magnetic tower jets in the laboratory. in *Phys. Plasmas* (2007).

[21] B. Albertazzi, J. Béard, A. Ciardi, T. Vinci, J. Albrecht, J. Billette, T. Burris-Mog, S.N. Chen, D. Da Silva, S. Dittrich, T. Herrmannsdörfer, B. Hirardin, F. Kroll, M. Nakatsutsumi, S. Nitsche, C. Riconda, L. Romagnagni, H.P. Schlenvoigt, S. Simond, E. Veuillot, T.E. Cowan, O. Portugall, H. Pépin and J. Fuchs. Production of large volume, strongly magnetized laser-produced plasmas by use of pulsed external magnetic fields. Rev. Sci. Instrum. **84**, (2013).

[22] A. Ciardi, T. Vinci, J. Fuchs, B. Albertazzi, C. Riconda, H. Pépin and O. Portugall. Astrophysics of Magnetically Collimated Jets Generated from Laser-Produced Plasmas. Phys. Rev. Lett. **110**, 025002 (2013).

[23] P.J. Armitage. Dynamics of Protoplanetary Disks. Annu. Rev. Astron. Astrophys. **49**, 195 (2011).

[24] C. Argiroffi, A. Maggio, G. Peres, J.J. Drake, J.L. Santiago, S. Sciortino and B. Stelzer. X-ray optical depth diagnostics of T Tauri accretion shocks. Astron. Astrophys. **507**, 939 (2009).

[25] R.L. Curran, C. Argiroffi, G.G. Sacco, S. Orlando, G. Peres, F. Reale and A. Maggio. Multi-wavelength diagnostics of accretion in an X-ray selected sample of CTTSs. Astron. Astrophys. **526**, 104 (2011).

[26] N.S. Brickhouse, S.R. Cranmer, A.K. Dupree, G.J.M. Luna and S. Wolk. A deep Chandra X-ray spectrum of the accreting young star TW Hydrae. Astrophys. J. **710**, 1835 (2010).